Korean J. Chem. Eng., 39(8), 2138-2147 (2022)
DOI: 10.1007/s11814-022-1074-7

pISSN: 0256-1115
eISSN: 1975-7220

Eco-friendly inorganic-organic bionanocomposite (Copper oxide - Carboxyl methyl cellulose - Guar gum): Preparation and effective removal of dye from aqueous solution

Ali Hosseinian Naeini*, Mohammadreza Kalaee*,,†, Omid Moradi***, Ramin Khajavi*, and Majid Abdouss****

*Department of Chemical and Polymer Engineering, South Tehran Branch, Islamic Azad University, Tehran, Iran
**Nanotechnology Research Centre, Tehran South Branch, Islamic Azad University, Tehran 15847-43311, Iran
***Department of Chemistry, Faculty of Science, Shahr-e-Qods Branch, Islamic Azad University, Tehran, Iran
****Department of Chemistry, Amirkabir University of Technology, Tehran 15875-4413, Iran
(*Received 22 October 2021 • Revised 18 January 2022 • Accepted 23 January 2022*)

Abstract−Biopolymers, such as Carboxyl methylcellulose (CMC) and Guar gum (GG), have attracted much attention. Herein, binary organic composite (Carboxyl methyl cellulose - Guar gum) and ternary inorganic-organic eco-friendly bionanocomposite (Copper oxide - Carboxyl methyl cellulose - Guar gum) with different wt% of CuO (1%, 3%, and 5% denoted as CMC/GG/CuO-1, CMC/GG/CuO-3, and CMC/GG/CuO-5) were prepared. The CMC, GG, CuO, CMC/GG, CMC/GG/CuO-1, CMC/GG/CuO-3, and CMC/GG/CuO-5 were characterized by XRD, FTIR, SEM, and EDX and used to remove malachite green (MG) dye from water. The effect of operational parameters on the adsorption process was investigated in detail. The maximum dye capacity was 18.5 mg/g. The isotherm data showed the Freundlich isotherm, which indicated the non-uniformity of adsorption on the adsorbent surface. Pollutant removal followed the pseudo-second-order kinetics. Also, the thermodynamic study presented that adsorption was spontaneous and endothermic.

Keywords: Eco-friendly Bionanocomposite, Binary Organic Composite, Ternary Inorganic-organic Composite, Malachite Green, Dye Removal

INTRODUCTION

Industrialization and population growth of the world has doubled the pressure on existing resources due to the limited resources of fresh and drinking water [1]. A wide range of compounds, including dyes, insecticides, petroleum products, paper, leather, plastics and rubber, detergents, oils, pharmaceutical, and personal care products compounds, exist in water sources [2]. Dyes have been widely considered and used in today's advanced industries and technologies. They cause many environmental problems due to the formation of strong, toxic, carcinogenic, mutagenic, and non-biodegradable species [3,4]. Organic dyes are chemically stable and can appear as anionic, cationic, or non-ionic due to their complex aromatic structures [5]. Malachite green (MG) is a cationic dye that is widely utilized in different industries, including leather, silk, cotton, wool, and paper. The discharge of organic dyes in aquatic ecosystems adversely affects aquatic species [6,7]. They reduce the penetration of sunlight and affect the photosynthetic activities of aquatic animals [8]. Therefore, an effective, efficient, and economical process to reduce the concentration of organic pollutants before release into the aquatic environment is needed [9,10]. For this purpose, conventional physical and physicochemical methods, including adsorption, biological oxidation, ultrafiltration, membrane, photocatalysis, ion exchange, and chemical coagulation, have been utilized to separate and eliminate pollutants from effluents [11-14]. Among the mentioned methods, the adsorption process is one of the most common procedures due to its high efficiency, economy, and simplicity of work [15]. Many researchers focus on using adsorbents based on nanomaterials (copper oxide, graphene oxide, etc.) with biodegradable polymer compounds with high adsorption capacity and low cost, including chitin, alginate, guar gum, and carboxymethylcellulose [16-19].

Cellulose is a linear polymer with high molecular weight that is natural, renewable, and biodegradable with high crystallinity and strong intramolecular hydrogen bonding that is not soluble in most organic solvents [20,21]. The conversion of cellulose to its derivatives such as carboxymethylcellulose (CMC) based on the Williamson ether reaction is a way to increase the efficiency of cellulose [22,23]. CMC with long chain, anionic and water-soluble properties was first produced from linear polysaccharide biopolymers in 1918 [24,25]. It has been considered as an alternative to synthetic polymers due to its cheapness, non-toxicity, production of transparent films, high viscosity, biodegradable and biocompatible. CMC has a variety of applications in various fields including textiles, paper, food, detergents, cosmetics, and pharmaceutical industries [23,26].

Guar gum (GG) is cheap, non-toxic, biodegradable, and prone to microbial degradation of natural polysaccharides that have shown the ability to effectively adsorb various pollutants. GG is known as

†To whom correspondence should be addressed.
E-mail: mohammad.kalaee@gmail.com, mr_kalaee@azad.ac.ir

Gavar, Guwar, bean Guyan, Guaran, Glucotard, Cuarina, Cyamopsis, Cluster bean powdered endosperm of Cyamopsis tetragonolobus seeds [27,28]. Chemically, GG is a natural non-ionic complex polysaccharide composed of the sugars galactose and mannose [29, 30]. It is a substance with effective and unique properties, including film-forming, viscous and concentration-enhancing agent, adhesive agent, gelling, and even wound healing agent. GG is also used in various industries, including food, textile, paint and coating, agriculture, pharmaceutical, and personal care products [31,32].

Metal oxides are used to improve or develop the functional properties of polymers. Copper oxide (CuO) nanoparticles have significant antimicrobial performance and semiconductor properties due to their specific and unique crystal structure. They are widely used for various applications in fields such as magnetic storage devices, catalysts, ceramics, thermal sensors, and superconducting materials.

Adsorption of dyes by different adsorbents including CMC/g-C_3N_4/ZnO [33], CGOA [34], CA [35], CGAs [36], and CMC/GOCOOH [37] was carried out. A literature review indicated that ternary inorganic-organic eco-friendly bionanocomposite (Carboxyl methylcellulose (CMC) - Guar gum (GG) - Copper oxide (CuO)) with different wt% of CuO was not used to remove dye from water. In the present study, inorganic-organic nanocomposite (CMC/GG/CuO) with different wt% of CuO (1%, 3%, and 5% denoted as CMC/GG/CuO-1, CMC/GG/CuO-3, and CMC/GG/CuO-5) were prepared and used to remove malachite green (MG) dye. Important parameters such as adsorbent amount, temperature, pH, contact time, and initial dye concentration on the removal efficiency of contaminant from water were investigated. Also, adsorption isotherm, kinetic, and thermodynamic were investigated in detail.

EXPERIMENTAL

1. Materials

Copper oxide (CuO), Guar gum (GG), carboxymethylcellulose (CMC), and Malachite green (MG) (Mw=364.9 g/mol, $C_{23}H_{25}ClN_2$) were procured from Sigma-Aldrich. The chemical structure of Malachite green is illustrated in Fig. 1. Dilute HCl and NaOH were utilized to regulate the pH of the pollutants solution.

2. Synthesis

2-1. CMC/GG Nanocomposite

1 g of CMC was added into 100 mL of deionized water at room temperature under intense magnetic stirring for 1 h. Then 1 g GG was added to the CMC solution. The resulting mixture was subjected to intense stirring for 3 h for complete dissolution. The prepared CMC/GG composite was dried at room temperature.

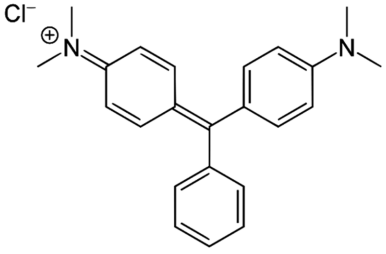

Fig. 1. The chemical structure of malachite green.

2-2. CMC/GG/CuO Nanocomposite

To synthesize the biopolymer/nanoparticle nanocomposite, 1 g of CMC was added to 100 mL of deionized water and subjected to intense stirring for 1 h. Then 1 g of GG was added to the above-mentioned solution; different wt% of CuO (1, 3, and 5%) was gently added to the mixture containing CMC/GG. The resulting mixture was continuously stirred vigorously for 3 h for complete and uniform dissolution. The prepared CMC/GG/CuO composites (with different wt% of CuO including 1, 3, and 5% denoted as CMC/GG/CuO-1, CMC/GG/CuO-3, and CMC/GG/CuO-5) were dried at room temperature.

3. Characterization

The FT-IR (Perkin Elmer) was utilized to identify the functional groups of biopolymers and the prepared nanocomposite materials in the range of 450-4,000 cm^{-1}. X-ray diffraction (XRD) was used to record the crystalline nature of the samples using an X-ray Diffractometer. To investigate the morphology of materials, scanning electron microscopy (SEM) (VEGA3) was utilized. The UV/Vis spectrophotometer (Lambda-25 Perkin Elmer) was used to measure dye concentration.

4. Dye Adsorption

The adsorption experiments of malachite green dye in 100 mL of solution were investigated using biopolymers and nanocomposites as adsorbents. Dye solution with a specific initial concentration (20 mg/L) was prepared and its pH was adjusted using HCl and NaOH in the range of 3.5 to 6.5. Then, by adding 0.1 g of adsorbent to the solution, it was stirred for 90 min at ambient temperature and sample solutions were taken at specified time intervals for determining dye concentration by a spectrophotometer at the maximum wavelength of dye (617 nm). The dye removal percentage and adsorption capacity (q_t: mg/g at time t and the adsorption capacity at equilibrium (q_e)) were evaluated from Eqs. (1), (2), respectively:

$$R\% = \frac{(C_0 - C_t)}{C_0} * 100 \quad (1)$$

$$q_e = \frac{(C_0 - C_e)V}{m} \quad (2)$$

RESULTS AND DISCUSSION

1. Characterization

1-1. FTIR

To understand the chemical nature and identify the functional groups of the materials used, FTIR analysis was performed. Fig. 2 shows the FTIR spectrum of CuO, GG, CMC, CMC/GG, CMC/GG/CuO-1, CMC/GG/CuO-3 and CMC/GG/CuO-5 in the 4,000 to 450 cm^{-1}. For CuO nanoparticles, the characteristic bands observed in 3,478, 3,390, and 1,624 cm^{-1} can be related into symmetric stretching vibrations of the O-H bond and asymmetric O-H bond, bending vibration of O-H. Also, the peaks observed in the vibrational state of the water molecule and the peaks of 613 and 502 cm^{-1} are attached to the vibrational states of the Cu-O bond. In the GG spectrum, the band at 3,413 cm^{-1} is related to the O-H stretching vibrations and the band 2,915 cm^{-1} is related to the C-H stretching vibration. While the bands observed in 1,618, 1,418,

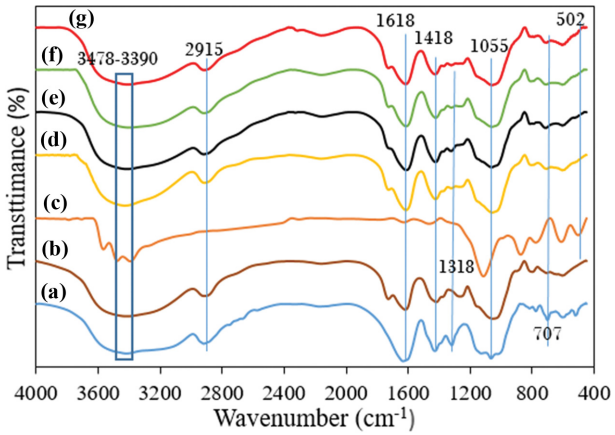

Fig. 2. FTIR spectra (a) CMC; (b) GG; (c) CuO; (d) CMC/GG; (e) CMC/GG/CuO-5; (f) CMC/GG/CuO-1; (g) CMC/GG/CuO-3.

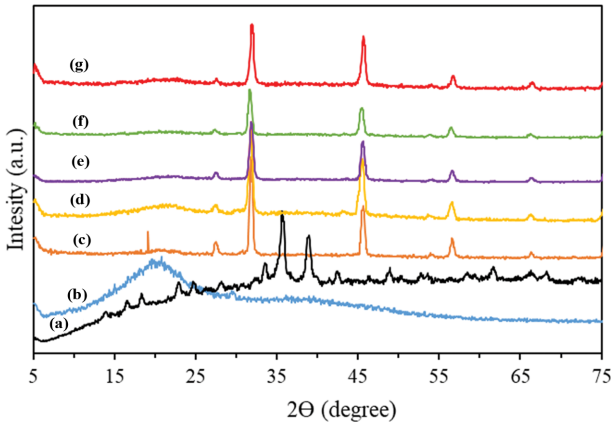

Fig. 3. XRD pattern (a) CuO; (b) GG; (c) CMC; (d) CMC/GG; (e) CMC/GG/CuO-5; (f) CMC/GG/CuO-1; and (g) CMC/GG/CuO-3.

and 1,055 cm^{-1} are attached to the cyclic stretching of galactose and mannose, the C-H bending vibration, and the O-H bending vibration, respectively. Weak strips of about 707 cm^{-1} are due to ring tension and ring deformation of the joints. Similarly, the FTIR spectrum of CMC is shown in Fig. 2. As we can see from Fig. 2, the wide bands at 3,417 and 2,918 cm^{-1} correspond to the O-H tensile band and the C-H stretching vibration, respectively. The bands appearing in 1,632, 1,418, 1,318, and 1,066 cm^{-1} are attributed to the stretching vibration of the carboxyl groups, C-H deformation, C-O stretching, and C-O-C stretching, respectively.

1-2. XRD

Fig. 3 shows the XRD patterns of CuO, GG, CMC, and nanocomposites of CMC/GG/CuO. The results are in good accord with the results of previous sources. The XRD pattern of the samples with an angle of 2θ in the range of 5°-75° is shown in Fig. 3. The XRD pattern confirms that CuO nanoparticles have a monoclinic and crystalline structure with characteristic peaks of 33.5°, 35.65°, 38.9°, 48.83°, 53.61° and 61.75°. The characteristic peak of GG at 20.06° indicates that it has extensive polymer networks. The XRD pattern of CMC with characteristic peaks of 19.15°, 27.55°, 31.75°, 45.65° and 56.71° with an angle of 2θ shows a crystalline structure. The XRD pattern shows that increasing the weight percentage of CuO-NPs in the CMC/GG/CuO matrix reduces the peak intensity. Also, CMC/GG/CuO biopolymer nanocomposite has a monoclinic structure.

Table 1. EDX analysis of CuO, CMC, GG, and CMC/GG/CuO-3

Sample	Element	wt %	Atomic %
CuO	C	7.95	18.91
	O	29.74	53.08
	Cu	62.31	28.01
CMC	C	39.15	46.15
	O	60.85	53.85
GG	C	39.87	46.90
	O	60.13	53.10
CMC/GG/CuO-3	C	28.99	37.85
	O	60.85	59.65
	Cu	10.16	2.51

1-3. SEM

The surface morphology of the materials was determined utilizing SEM images. The images are illustrated in Fig. 4. As can be seen from Fig. 4(a), CuO nanoparticles have a monodisperse morphology with a distinct crystalline structure and are almost uniform in that the diameter of CuO nanoparticles varies from 30 to 50 nm. The SEM image of the CMC biopolymer shows an irregular shape and an uneven surface (Fig. 4(b)). GG image has cavities, layers, and heterogeneous appearance (Fig. 4(c)). CMC/GG/CuO-3 nanocomposite is a porous and layered material (Fig. 4(d)). CuO nanoparticles are also clearly visible on the CMC/GG/CuO composite, indicating that the CuO has been successfully loaded on the CMC/GG composite.

1-4. EDX

EDX was performed to investigate the chemical properties of the used materials. Table 1 shows the results of EDX. According to Table 1, the main chemical elements, namely C, O, and Cu, are visible and no impurities from the composition of other elements are visible.

2. Pollutant Removal

2-1. Effect of CuO wt%

The effect of different wt% of CuO (1, 3, 5%) in CMC/GG/CuO nanocomposite on the dye removal at room temperature was studied to optimize it. According to the results shown in Fig. 5, by changing the wt% of CuO, the adsorption capacity changes significantly. As can be seen, the 3 wt% has a higher adsorption capacity than the other two values. Increasing wt% of CuO causes blockage of pores and pores of biopolymer nanocomposites. Therefore, the optimal wt% of CuO on CMC/GG biopolymers was selected to be 3 wt%.

2-2. Initial Concentration

The contaminant concentration is one of the most important parameters of pollutant removal [38-42]. The impact of initial dye concentration on the adsorption of MG with the prepared adsorbents was studied. The amount of 0.1 g of adsorbent was determined in 100 mL of dye solution at various concentrations (20, 30,

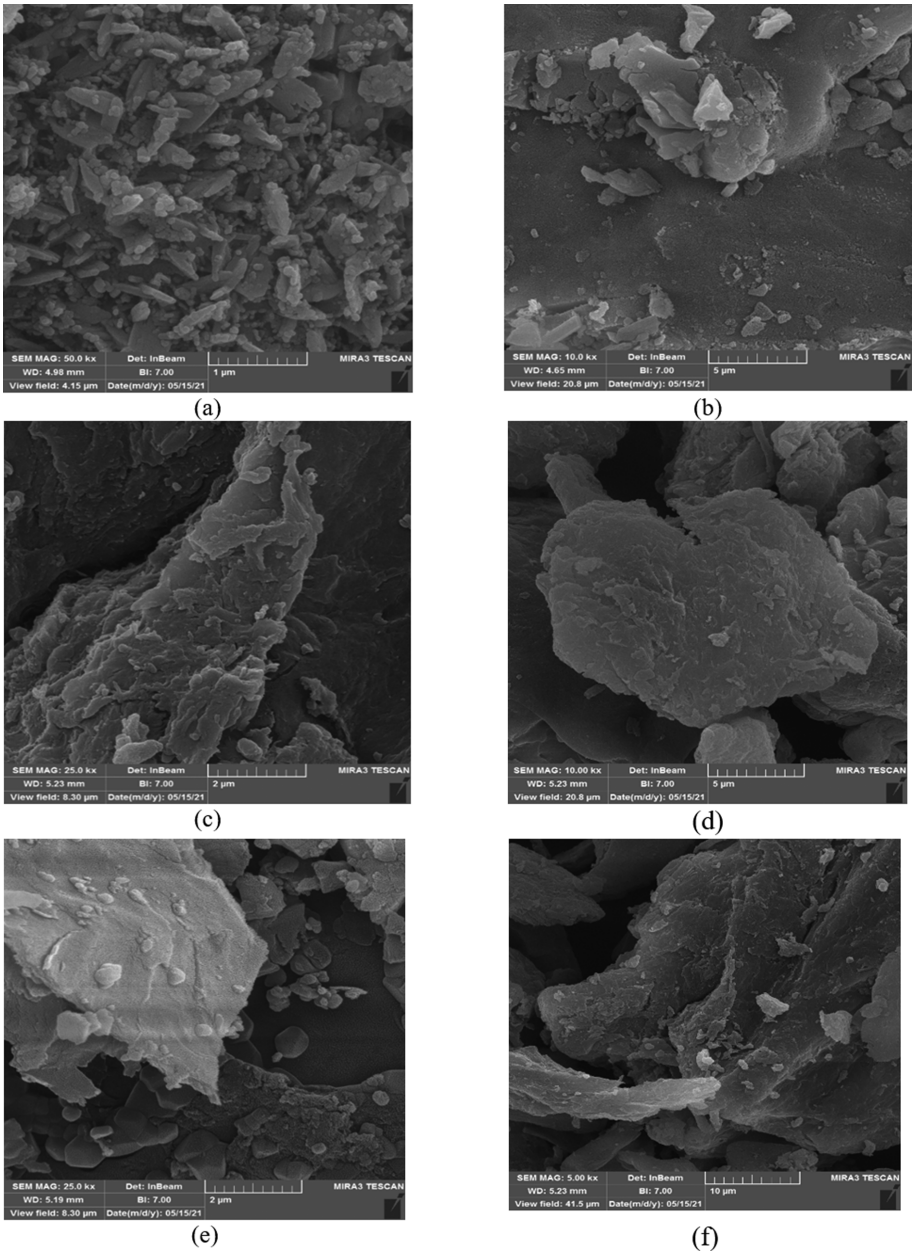

Fig. 4. SEM images (a) CuO, (b) CMC, (c) GG, and (d) CMC/GG/CuO-1, (e) CMC/GG/CuO-3, and (f) CMC/GG/CuO-5.

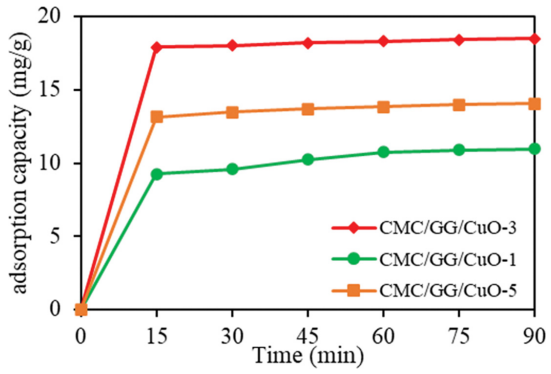

Fig. 5. Impact of different ratios (1, 3, and 5 wt%) CMC/GG/CuO on the adsorption capacity.

40, and 50 mg/L) and with optimal pH adjustment (6.5). Approximately 89% dye removal occurs with an initial concentration of 20 mg/L in the first 15 min of the process. According to Fig. 6, with increasing the concentration of dye solution, the percentage of dye removal decreased [43]. The final amount of removal efficiency 92.4% and the amount of adsorption capacity 18.5 mg/g were obtained. The dye removal efficiency of CMC/GG/CuO-3 with different concentrations of 20, 30, 40 and 50 mg/l is 92.4%, 75.1%, 61.3% and 43.6%, respectively. Also, the dye removal efficiency of CMC/GG with different concentrations of 20, 30, 40 and 50 mg/l is 64%, 55.5%, 43.3% and 36.1%, respectively. By increasing the concentration of dye, repulsion is created between the dye molecules and they are prevented from being adsorbed by the adsorbent [43,44].

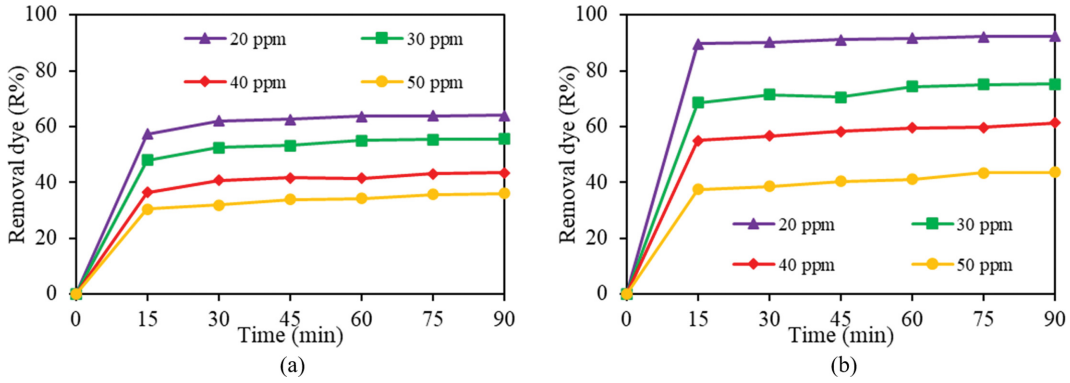

Fig. 6. Effect of initial concentration pollutants (20, 30, 40 and 50 mg/L) (a) CMC/GG; (b) CMC/GG/CuO-3 on dye MG.

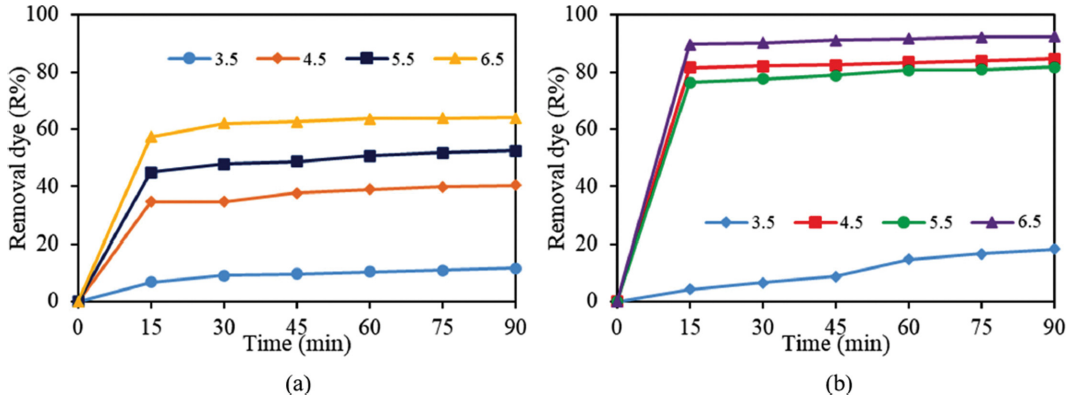

Fig. 7. Effect of pH on MG removal (a) CMC/GG; (b) CMC/GG/CuO-3.

2-3. pH

To study the efficacy of pH on the adsorption of MG with biopolymer adsorbents, a dye solution with an initial concentration (20 mg/L) and optimal adsorbent dosage of 0.1 g was prepared and their pH was adjusted by HCl and NaOH in different pH ranges from 3.5 to 6.5. The results of this investigation are illustrated in Fig. 7. The maximum removal efficiency (92.4%) of MG was observed at pH=6.5. The MG is positively charged when dissolved in water. Thus, by lowering the pH (in an acidic environment), the number of positively charged sites increases and the removal efficiency decreases. As can be seen, when the pH of the solution is increased from 3.5 to 6.5, the adsorbent surface becomes negatively charged and therefore increases the removal efficiency of MG due to the increased electrostatic attraction between the positively charged cationic dye and the negatively charged biopolymer adsorbent [7, 19,45].

2-4. Contact Time

Effect of contact time on MG adsorption on CMC/GG and CMC/GG/CuO-3 biopolymer adsorbents in the range of 0-90 min (initial dye concentration: 20 mg/L, the amount of adsorbent: 0.1 g and pH: 6.5) was studied at room temperature. The results of this research are exhibited in Fig. 8. The data show that the amount of MG adsorption capacity for adsorbent CMC/GG (12.8 mg/g) and CMC/GG/CuO-3 (18.4 mg/g) increases with increasing contact time. Dye ions have more time to bind to active adsorption sites on the adsorbent surface. For this reason, the adsorption capacity initially increases rapidly and then slows. Further slowing of the adsorption rate is due to the gradual saturation of the adsorption active sites by the dye molecules, so increasing the contact time will not affect the adsorption capacity. Therefore, the final contact time for all experiments was 90 min [46-48].

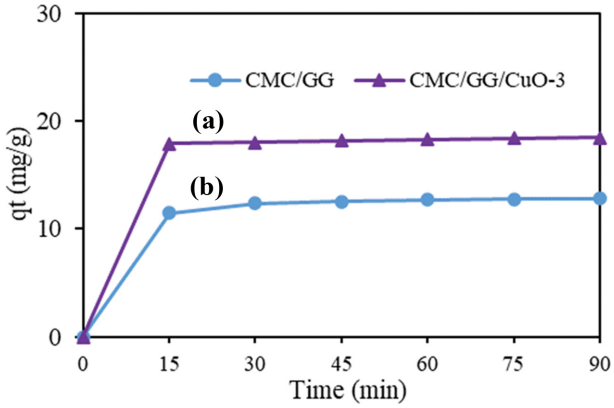

Fig. 8. Effect of contact time (15-90 min) (a) CMC/GG; (b) CMC/GG/CuO-3 on dye MG.

2-5. Dosage

Adsorption of MG on CMC/GG and CMC/GG/CuO biopolymer nanocomposite adsorbents by changing the amount of adsorbent from 0.05 g to 0.1 g (room temperature, initial dye concen-

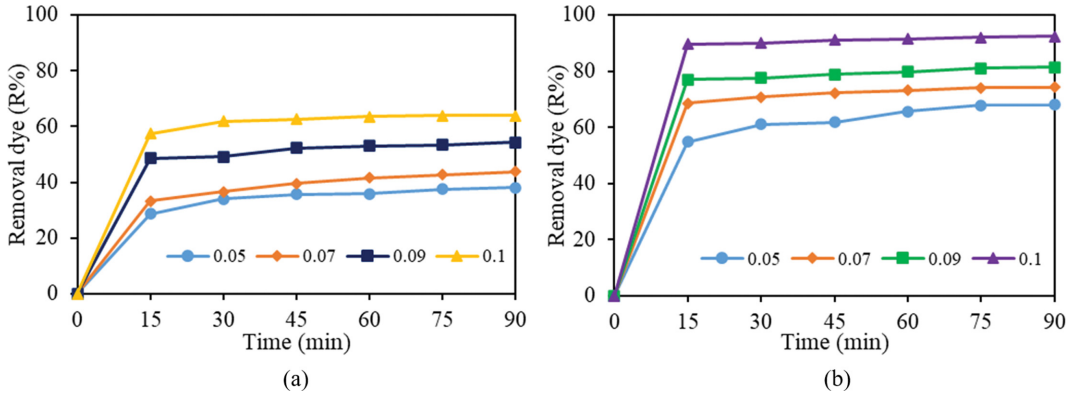

Fig. 9. Effect of adsorbent dosage (5, 7, 9, and 10 mg) on MG removal (a) CMC/GG, and (b) CMC/GG/CuO-3.

tration 20 mg/l and pH 6.5) was studied. According to the results observed in Fig. 9, by increasing the amount of adsorbent from 0.05 to 0.1 g, the adsorption percentage increases significantly; this increases the desired level of adsorbent and the availability of more active adsorption sites for adsorption. By changing the amount of adsorbent from 0.05-0.1 g, the percentage of dye removal increases significantly (from 67.6 to 92.4%). The dye removal efficiency of CMC/GG/CuO-3 with different dosages of 0.05, 0.07, 0.09 and 0.1 g is 67.9%, 74.2%, 81% and 92.4%, respectively. The dye removal efficiency of CMC/GG with different dosages of 0.05, 0.07, 0.09 and 0.1 g is 38.03%, 43.7%, 54.4% and 64%, respectively. Therefore, 0.1 g was selected as the optimal adsorbent dose for all experiments. As shown in Fig. 9, with increasing the adsorbent dosage, the dye removal was increased effectively due to the increased adsorption surface sites. Indeed, adsorption capacity is directly affected by the number of active sites [49,50].

2-6. Adsorption Isotherms

Isotherm investigates the relationship between the concentration of adsorbate in solution and on the adsorbent surface chemically or physically at a constant temperature. In this way, the adsorption capacity of the adsorbent in equilibrium is determined with the help of special constants that indicate the surface properties as well as the adsorbent tendency to adsorb the contaminant. The linear equation for the Langmuir and Freundlich isotherms is given in Eqs. (3), and (4), respectively [51-54]:

$$\frac{C_e}{q_e}=\frac{1}{K_L}\cdot q_l+\frac{C_e}{q_l} \tag{3}$$

$$\log q_e=\log K_f+\frac{1}{n}\log C_e \tag{4}$$

In these relations, C_e is the concentration of dye in equilibrium (mg/L) and q_e is the amount of adsorbed material per adsorbent mass in equilibrium (mg/g). q_l is the maximum amount of adsorbed material per adsorbent mass (mg/g). The K_f and n are the Freundlich constants.

The Temkin isotherm examines the interaction between the adsorbent and the adsorption of the substance.

$$q_e=B_1\ln K_T+B_1\ln C_e \tag{5}$$

In this equation, B_1 (RT/b) is the Temkin constant, which represents the heat of adsorption and K_T is the equilibrium constant corre-

Table 2. Adsorption isotherm parameters of CMC/GG and CMC/GG/CuO-3 nanocomposite

Isotherm	Parameter	Adsorbents	
		CMC/GG	CMC/GG/CuO-3
Langmuir $C_e/q_e=1/K_L\ q_L+C_e/q_L$	q_L	18.41	12.69
	K_L	0.25	1.61
	R^2	0.7598	0.9913
Freundlich $\log q_e=\log K_F+1/n \log C_e$	K_F	7.60	20.40
	n	4.19	4.98
	R^2	0.3122	0.9437
Temkin $q_e=B_1 \ln K_T+B_1 \ln C_e$	K_T	5.35	493.35
	B_1	3.31	3.23
	R^2	0.32	0.9629

K_T; Equilibrium binding constant (L/g), C_e; Equilibrium dye concentration (mg/L), K_F; Freundlich constant (L/mg), K_L; Langmuir constant (L/g), n; the Freundlich intensity parameter (dimensionless), q_e; the amount of adsorbate uptake at equilibrium (mg/g), q_L (mg/g); the maximum adsorption capacity (mg/g) and R^2; Regression coefficient

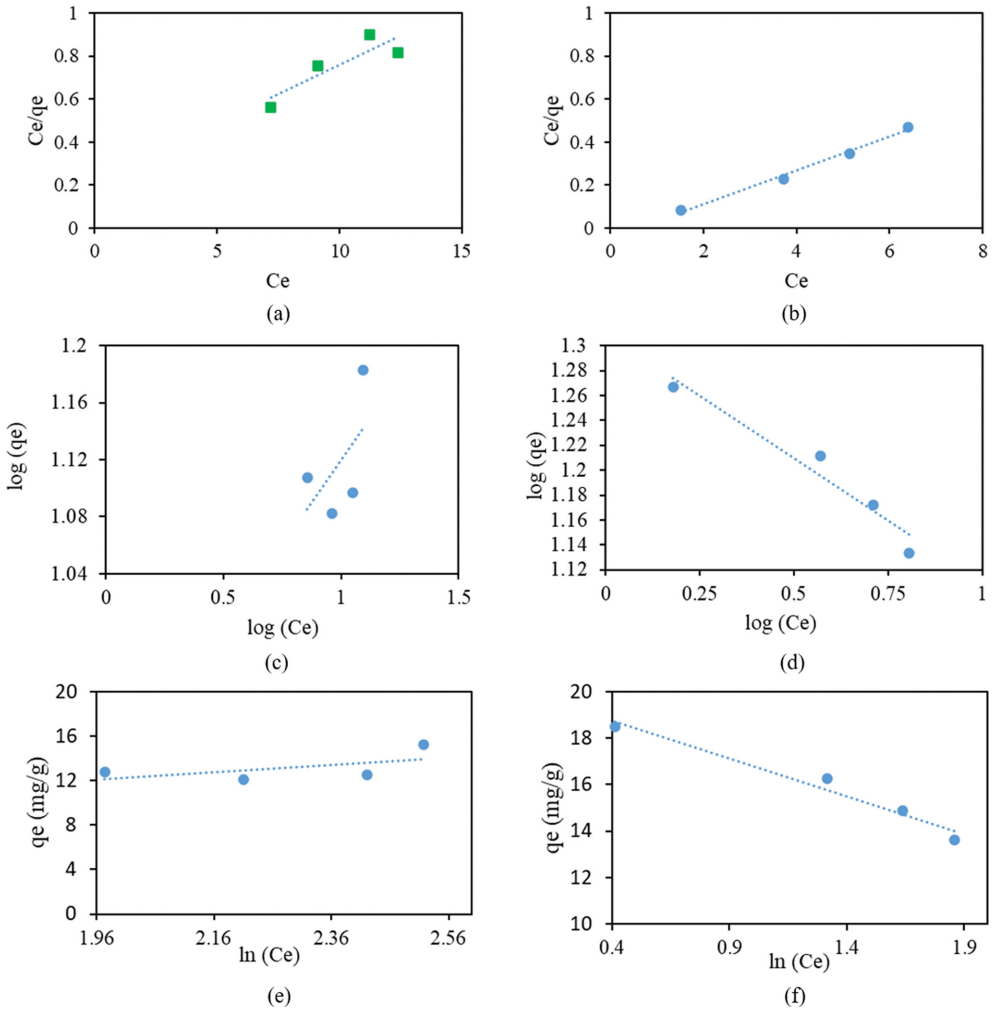

Fig. 10. The Langmuir isotherm ((a) CMC/GG and (b) CMC/GG/CuO-3), the Freundlich isotherm ((c) CMC/GG, and (d) CMC/GG/CuO-3) and the Temkin isotherm ((e) CMC/GG and (f) CMC/GG/CuO-3) of MG removal.

sponding to the maximum energy band (L/mg).

In this research, the Langmuir, Freundlich, and Temkin isotherms were utilized. Fig. 10 shows the results of the isotherm study in the MG adsorption using CMC/GG and CMC/GG/CuO. Table 2 presents the results of data analysis using the isotherm models with the mentioned adsorbents. The value obtained for the R^2 of each isotherm with the adsorbents indicates that MG removal by the adsorbents follows the Langmuir isotherm.

2-7. Adsorption Kinetics

The adsorption kinetics investigates the relationship between the reaction rate and the interactions between the adsorbate and the adsorbent [53,55-57]. The linear equations of the pseudo-first-order and pseudo-second-order models are as Eqs. (6) and (7), respectively:

$$\log(q_e - q_t) = \log q_e - (k_1/2.303)\cdot t \quad (6)$$

$$\frac{t}{q_t} = \frac{1}{k_2 q_e^2} + \frac{t}{q_e} \quad (7)$$

where k_1 (min^{-1}) and k_2 (g/mg·min) are the pseudo-first-order and pseudo-second-order adsorption equilibrium rate constants, respectively. Also, q_e is the amount of material adsorbed per unit mass in equilibrium, and q_t (mg/g) is the amount of capacity of the adsorbed material at the time (t).

A linear form of intraparticle diffusion models is (Eq. (8)):

$$q_t = k_p t^{1/2} + I \quad (8)$$

where q_t (mg/g), k_p (mg/g·$min^{0.5}$), and I (mg/g), are dye adsorption capacity at time t, rate constant, and intercept, respectively.

Using equilibrium data of adsorption, the kinetics of the reaction and its degree of agreement with the equations were investigated. Fig. 11 exhibits the results of pseudo-first-order, pseudo-second-order, and intraparticle kinetics of MG adsorption using CMC/GG and CMC/GG/CuO. Table 3 presents the results of data fitting on the kinetic models of the mentioned adsorbents. According to the values of R^2 (correlation coefficient) obtained for kinetic models, MG removal by CMC/GG and CMC/GG/CuO follows the pseudo-second-order model.

2-8. Adsorption Thermodynamics

Determination of thermodynamic parameters to remove MG at

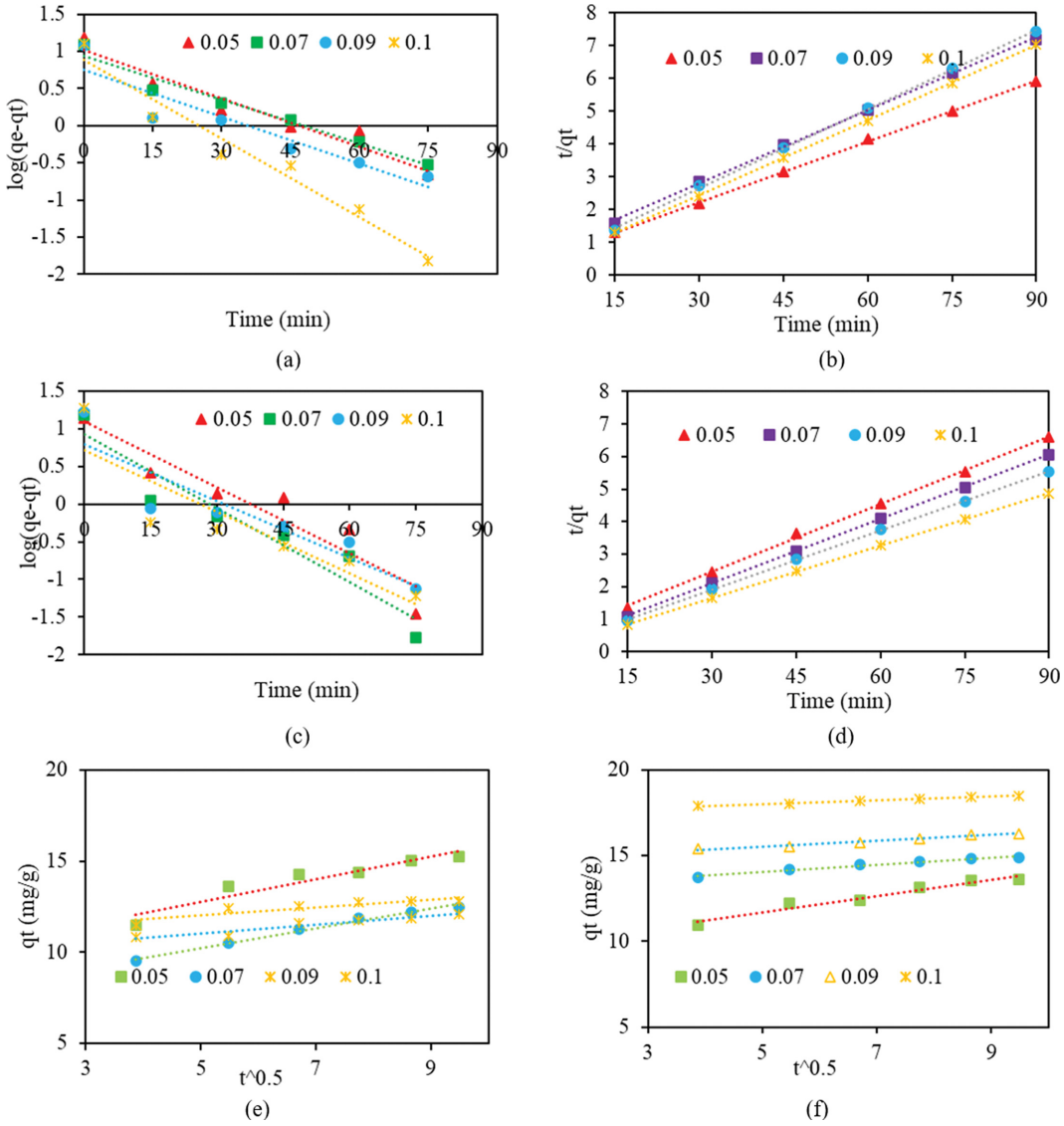

Fig. 11. The pseudo-first order ((a) CMC/GG; (b) CMC/GG/CuO-3), the pseudo-second order ((c) CMC/GG; (d) CMC/GG/CuO-3) and the Intraparticle diffusion kinetic ((e) CMC/GG; (f) CMC/GG/CuO-3) of MG removal.

Table 3. The kinetics coefficients of MG adsorption at different adsorbents doses

Adsorbent	Dose (g)	$(q_e)_{Exp}$	Pseudo-first-order			Pseudo-second-order			Intraparticle diffusion		
			$\log(q_e-q_t)=\log q_e-(k_1/2.303)\cdot t$			$t/q_t=1/k_2\cdot q_e^2+t/q_e$			$q_t=k_p\cdot t^{0.5}+I$		
			$(q_e)_{Cal.}$	k_1	R^2	$(q_e)_{Cal.}$	k_2	R^2	k_P	I	R2
CMC/GG	0.05	15.22	10.36	0.009	0.9392	16.20	0.009	0.9993	0.61	6.65	0.8968
	0.07	12.49	8.79	0.008	0.9636	13.44	0.009	0.9989	0.53	7.53	0.9873
	0.09	12.09	5.61	0.009	0.8720	12.45	0.024	0.9995	0.24	7.79	0.9335
	0.1	12.81	7.62	0.015	0.9623	13.01	0.039	1	0.21	10.92	0.8199
CMC/GG/CuO-3	0.05	13.59	12.24	0.012	0.8960	14.40	0.012	0.9987	0.47	9.34	0.9544
	0.07	14.85	8.39	0.014	0.9101	14.42	0.012	0.9999	0.21	13.01	0.9691
	0.09	16.27	6.21	0.011	0.8403	16.52	0.035	0.9998	0.16	14.68	0.9676
	0.1	18.50	5.11	0.011	0.8054	18.62	0.061	1	0.11	17.48	0.9878

k_1; Pseudo-first order rate constant (1/min), k_2; Pseudo-second order rate constant (g/mg min), k_p; Intraparticle diffusion rate constant (mg/g $min^{0.5}$), q_e; the amount of adsorbate uptake at equilibrium (mg/g), q_t; the amount of absorption at time t (mg/g), R^2; Regression coefficient, I; Intercept

Table 4. Thermodynamic parameters of adsorption by the adsorbent at different temperatures

Adsorbent	ΔH^o (kJ/mol)	ΔS^o (j/mol)	ΔG^o (kJ/mol)			
			Temperature			
			25 °C	30 °C	35 °C	40 °C
CMC/GG/GO-3	38.33	146.16	−4.99	−6.25	−6.98	−7.17

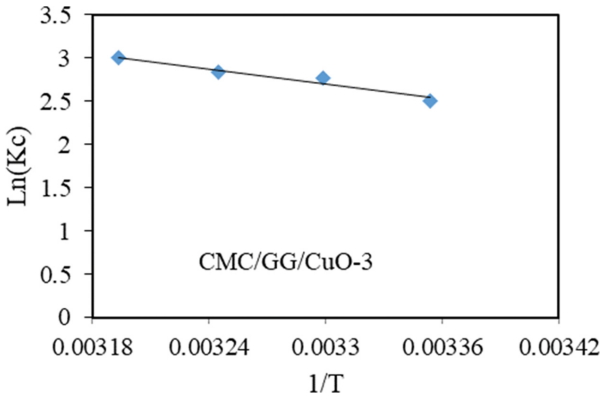

Fig. 12. Determination of thermodynamic parameters on adsorbent CMC/GG/CuO-3.

different temperatures of 25 °C, 30 °C, 35 °C, and 40 °C under optimal conditions (0.1 g of adsorbent, 100 mL of dye solution at an initial concentration of 20 mg/L at pH=6.5) was studied. Thermodynamic parameters can be calculated using Eqs. (9)-(11) [58-60]:

$$K_c = \frac{q_e}{C_e} \tag{9}$$

where K_c (L/g) is the equilibrium constant, C_e (mg/L) is the equilibrium concentration of the adsorbent in solution, and q_e (mg/g) is the amount of adsorbate on the adsorbent in equilibrium.

$$\mathrm{Ln}K_c = \left(\frac{\Delta S^o}{R}\right) - \left(\frac{\Delta H^o}{RT}\right) \tag{10}$$

where R is the global constant of gases (8.314 j/mol k) and T (K) is the absolute temperature.

$$\Delta G^o = \Delta H^o - T\Delta S^o \tag{11}$$

The thermodynamic parameters of MG adsorption on CMC/GG/CuO-3 biopolymer adsorbent are presented in Fig. 12. Since the penetration rate of dye molecules is under temperature control, temperature change can affect the equilibrium capacity of the adsorbent. Thermodynamic variables, ΔG^o (kJ/mol), ΔH^o (kJ/mol), and ΔS^o (J/mol K), are presented in Table 4. According to the results reported in Table 4, the negative free energy changes of the ΔG^o for the adsorbent indicate that the adsorption process is spontaneous. Also, the positive ΔH^o and the ΔS^o of the reaction indicate endothermic adsorption and the increase of irregularities in the adsorbent/solution interface, respectively [56,61]. According to the mentioned results, it can be said that the change and increase of irregularity in the structure of CMC/GG/CuO-3 biopolymer nanocomposite occurs in the adsorption process.

Various adsorbents, such as magnetic multiwall carbon nanotube nanocomposite (Methylene blue - adsorption capacity: 12 mg/g and Brilliant cresyl blue - adsorption capacity: 6 mg/g) [62], Magnetic alginate bead Methylene blue - adsorption capacity: 9 mg/g) [63], Zeolite (Maxilon Goldgelb GL EC - adsorption capacity: 15 mg/g) [64], Clay (Turkey) (Basic blue 9 - adsorption capacity: 6 mg/g) [65] were used to remove dyes. The results indicate that the used adsorbent in this study has suitable adsorption capacity.

CONCLUSION

Binary (CMC/GG) and ternary inorganic-organic eco-friendly nanocomposites (CMC/GG/CuO) with different wt% of CuO (1%, 3%, and 5% denoted as CMC/GG/CuO-1, CMC/GG/CuO-3, and CMC/GG/CuO-5) were prepared. The CMC, GG, CuO, CMC/GG, CMC/GG/CuO-1, CMC/GG/CuO-3, and CMC/GG/CuO-5 were characterized and used to remove malachite green (MG). The effect of operational parameters on the adsorption process was investigated in detail. The removal efficiency was 92.4% at the optimal amount of adsorbent=0.1 g with an initial concentration of dye of 20 mg/L and pH of 6.5 and within 90 min. The isotherm data indicated the Langmuir isotherm with the uniform of adsorption on the adsorbent surface. The MG removal obeyed pseudo-second-order kinetics. Thermodynamic data presented that MG removal was spontaneous and endothermic. The nanocomposite is biodegradable, biodegradable and biocompatible, and has also shown significant efficacy in removing malachite green dye. It can be said to be effective in reducing environmental pollution.

REFERENCES

1. N. M. Mahmoodi and M. Arami, *Chem. Eng. J.*, **146**, 189 (2009).
2. S. Davarpanah, N. M. Mahmoodi, M. Arami, H. Bahrami and F. Mazaheri, *Appl. Surf. Sci.*, **255**, 4171 (2009).
3. N. M. Mahmoodi and J. Abdi, *Microchem. J.*, **144**, 436 (2019).
4. S. Kashefi, S. M. Borghei and N. M. Mahmoodi, *J. Mole. Liq.*, **276**, 153 (2019).
5. N. Nasrollahi, S. Aber, V. Vatanpour and N. M. Mahmoodi, *Mater. Chem. Phys.*, **222**, 338 (2019).
6. N. T. T. Mai, N. K. Nga, D. T. M. Hue, T. N. Dung, H. D. Chinh and T. Q. Huy, *Adsorp. Sci. Technol.*, **2021**, 9193052 (2021).
7. N. K. Nga, N. T. T. Chau and P. H. Viet, *J. Sci. Adv. Mater. Dev.*, **5**, 65 (2020).
8. N. M. Mahmoodi, *Fib. Polym.*, **15**, 273 (2014).
9. J. Abdi, N. M. Mahmoodi, M. Vossoughi and I. Alemzadeh, *Micropor. Mesopor. Mater.*, **273**, 177 (2019).
10. Z. Yang, H. Peng, W. Wang and T. Liu, *J. Appl. Polym. Sci.*, **116**, 2658 (2010).
11. N. M. Mahmoodi, N. Y. Limaee, M. Arami, S. Borhany and M.

Mohammad-Taheri, *J. Photochem. Photobiol. A: Chem.*, **189**, 1 (2007).
12. N. M. Mahmoodi and M. H. Saffar-Dastgerdi, *Appl. Catal. B Environ.*, **268**, 118443 (2019).
13. N. M. Mahmoodi, M. Taghizadeh, A. Taghizadeh, J. Abdi, B. Hayati and A. A. Shekarchi, *Appl. Surf. Sci.*, **480**, 288 (2019).
14. N. M. Mahmoodi, *J. Environ. Eng.*, **139**, 1368 (2013).
15. N. M. Mahmoodi and M. H. Saffar-Dastgerdi, *Microchem. J.*, **145**, 74 (2019).
16. N. M. Mahmoodi, B. Hayati and M. Arami, *J. Chem. Eng. Data*, **55**, 4638 (2010).
17. Q. Kong, X. Wang and T. Lou, *Carbohydr. Polym.*, **244**, 116481 (2020).
18. V. Kanikireddy, K. Varaprasad, M. S. Rani, P. Venkataswamy, B. J. Mohan Reddy and M. Vithal, *Carbohydr. Polym.*, **236**, 116053 (2020).
19. N. M. Mahmoodi and Z. Mokhtari-Shourijeh, *Fib. Polym.*, **16**, 1861 (2015).
20. K. Hattori, E. Abe, T. Yoshida and J. A. Cuculo, *Polym. J.*, **36**, 123 (2004).
21. P. Rachtanapun, *Kasetsart J. - Nat. Sci.*, **43**, 259 (2009).
22. C. J. Tijsen, H. J. Kolk, E. J. Stamhuis and A. A. C. M. Beenackers, *Carbohydr. Polym.*, **45**, 219 (2001).
23. R. K. Singh and A. K. Singh, *Waste Biomass Valor.*, **4**, 129 (2013).
24. A. Bono, P. H. Ying, F. Y. Yan, C. L. Muei, R. Sarbatly and D. Krishnaiah, *Adv. Nat. Appl. Sci.*, **3**, 5 (2009).
25. J. V. Karabinos and M. Hindert, *Advances in carbohydrate chemistry*, Sincedirect (1954).
26. Z. Karimzadeh, S. Javanbakht and H. Namazi, *Bioimpacts*, **9**, 5 (2019).
27. R. Saxena and S. Sharma, *Int. J. Sci. Eng. Res.*, **7**, 675 (2016).
28. G. Sharma, S. Sharma, A. Kumar, A. H. Al-Muhtaseb, M. Naushad, A. A. Ghfar, G. T. Mola and F. J. Stadler, *Carbohydr. Polym.*, **199**, 534 (2018).
29. V. Jain, V. Tammishetti, K. Joshi, D. Kumar, Pradip and B. Rai, *Miner. Eng.*, **109**, 144 (2017).
30. D. Verma and S. K. Sharma, *Int. J. Biol. Macromol.*, **181**, 653 (2021).
31. N. Thombare, U. Jha, S. Mishra and M. Z. Siddiqui, *Int. J. Biol. Macromol.*, **88**, 361 (2016).
32. D. Mudgil, S. Barak and B. S. Khatkar, *J. Food Sci. Technol.*, **51**, 409 (2014).
33. G. Sharma, A. Kumar, S. Sharma, M. Naushad, A. A. Ghfar, A. H. Al-Muhtaseb, T. Ahamad, N. Sharma and F. J. Stadler, *Cellulose*, **27**, 3677 (2020).
34. Y. Lv, B. Xing, M. Zheng, G. Yi, G. Huang, C. Zhang, R. Yuan, Z. Chen and Y. Cao, *Nanomaterials*, **8**, 1 (2018).
35. N. S. V. Capanema, A. A. P. Mansur, H. S. Mansur, A. C. de Jesus, S. M. Carvalho, P. Chagas and L. C. de Oliveira, *Environ. Technol.*, **39**, 2856 (2018).
36. P. Pal, A. G. Corpuz, S. W. Hasan, M. Sillanpää and F. Banat, *Sep. Purif. Technol.*, **255**, 117684 (2021).
37. A. S. Eltaweil, G. S. Elgarhy, G. M. El-Subruiti and A. M. Omer, *Int. J. Biol. Macromol.*, **154**, 307 (2020).
38. N. M. Mahmoodi, M. Arabloo and J. Abdi, *Water Res.*, **67**, 216 (2014).
39. N. M. Mahmoodi, *Desalin. Water Treat.*, **53**, 84 (2015).
40. N. M. Mahmoodi and M. Arami, *J. Appl. Polym. Sci.*, **109**, 4043 (2008).
41. N. M. Mahmoodi, B. Hayati, M. Arami and F. Mazaheri, *J. Chem. Eng. Data*, **55**, 4660 (2010).
42. N. M. Mahmoodi, *J. Mole. Catal. A: Chem.*, **366**, 254 (2013).
43. N. M. Mahmoodi, *J. Environ. Eng.*, **139**, 1382 (2013).
44. T. A. Khan, M. Nazir, I. Ali and A. Kumar, *Arab. J. Chem.*, **10**, S2388N (2017).
45. L. G. T. dos Reis, N. F. Robaina, W. F. Pacheco and R. J. Cassella, *Chem. Eng. J.*, **171**, 532 (2011).
46. S. Abuzerr, M. Darwish and A. H. Mahvi, *Water Sci. Technol.*, **2017**, 534 (2017).
47. A. C. Tella, M. D. Olawale, M. Neuburger and J. A. Obaleye, *J. Solid State Chem.*, **255**, 157 (2017).
48. M. Ghaedi, A. Ansari, M. H. Habibi and A. R. Asghari, *J. Ind. Eng. Chem.*, **20**, 17 (2014).
49. K. Zare, H. Sadegh, R. Shahryari-Ghoshekandi, B. Maazinejad, V. Ali, I. Tyagi, S. Agarwal and V. K. Gupta, *J. Mol. Liq.*, **212**, 266 (2015).
50. N. Marsiezade and V. Javanbakht, *Int. J. Biol. Macromol.*, **162**, 1140 (2020).
51. N. M. Mahmoodi, *Water. Air. Soil Pollut.,* **224**, 1419 (2013).
52. N. M. Mahmoodi and F. Najafi, *Micropor. Mesopor. Mater.*, **156**, 153 (2012).
53. N. M. Mahmoodi, M. Oveisi, A. Taghizadeh and M. Taghizadeh, *J. Hazard. Mater.*, **368**, 746 (2019).
54. N. M. Mahmoodi, M. Oveisi, A. Taghizadeh and M. Taghizadeh, *Carbohydr. Polym.*, **227**, 115364 (2020).
55. M. Oveisi, N. M. Mahmoodi and M. A. Asli, *J. Clean. Prod.*, **222**, 669 (2019).
56. N. M. Mahmoodi, *J. Taiwan Instit. Chem. Eng.*, **45**, 2008 (2014).
57. H. Hoseinzadeh, B. Hayati, F. Shahmoradi, K. Seifpanahi-shabani and N. M. Mahmoodi, *Mater. Res. Bull.*, **142**, 111408 (2021).
58. J. Li, Z. Wu, Q. Duan, A. Alsaedi, T. Hayat and C. Chen, *J. Clean. Prod.*, **204**, 896 (2018).
59. S. Naeimi and H. Faghihian, *Environ. Toxicol. Pharmacol.*, **53**, 121 (2017).
60. B. N. Bhadra, D. K. Yoo and S. H. Jhung, *Appl. Surf. Sci.*, **504**, 144348 (2020).
61. Z. Inonu, S. Keskin and C. Erkey, *ACS Appl. Nano Mater.*, **1**, 5959 (2018).
62. S. Thurm and S. Odenbach, *J. Magn. Magn. Mater.*, **252**, 247 (2002).
63. J. Sun, R. Xu, Y. Zhang, M. Ma and N. Gu, *J. Magn. Magn. Mater.*, **312**, 354 (2007).
64. V. Meshko, L. Markovska, M. Mincheva and A. E. Rodrigues, *Water Res.*, **35**, 3357 (2001).
65. A. Gurses, S. Karaca, C. Dogar, R. Bayrak, M. Acıkyıldız and M. Yalcın, *J. Colloid Interface Sci.*, **269**, 310 (2004).